

CrystEngComm

Accepted Manuscript



This is an *Accepted Manuscript*, which has been through the Royal Society of Chemistry peer review process and has been accepted for publication.

Accepted Manuscripts are published online shortly after acceptance, before technical editing, formatting and proof reading. Using this free service, authors can make their results available to the community, in citable form, before we publish the edited article. We will replace this *Accepted Manuscript* with the edited and formatted *Advance Article* as soon as it is available.

You can find more information about *Accepted Manuscripts* in the [Information for Authors](#).

Please note that technical editing may introduce minor changes to the text and/or graphics, which may alter content. The journal's standard [Terms & Conditions](#) and the [Ethical guidelines](#) still apply. In no event shall the Royal Society of Chemistry be held responsible for any errors or omissions in this *Accepted Manuscript* or any consequences arising from the use of any information it contains.

Cite this: DOI: 10.1039/c0xx00000x

www.rsc.org/xxxxxx

ARTICLE TYPE

Hydrothermal Growth and Characterization of Length Tunable Porous Iron Vanadate One-dimensional Nanostructures

Lei Huang, Liyi Shi, Xin Zhao, Jing Xu, Hongrui Li, Jianping Zhang and Dongsong Zhang*

Received (in XXX, XXX) Xth XXXXXXXXXX 20XX, Accepted Xth XXXXXXXXXX 20XX

DOI: 10.1039/b000000x

A simple hydrothermal method was applied to controllably synthesize porous FeV_xO_y one-dimensional (1-D) nanostructures. The length of the 1-D nanostructures could be tuned from several micrometers to several millimeters. The formation process of the porous FeV_xO_y 1-D nanostructures can be summarized into four steps, namely dissolution, anisotropic growth, ostwald ripening and dehydration. It was found that the pore sizes decrease with the increase of pH values while the surface areas increase with the increase of pH values. Finally, the porous FeVO_4 nanorods were found very active and stable in the application of selective catalytic reduction of NO with NH_3 .

Introduction

Transition-metal vanadates nanostructures have recently attracted extensive attention attributed to their wide range of applications in high energy density lithium batteries, sensors and catalysis.¹⁻⁴ Vanadate 1-D nanostructures in the form of nanorods,⁵⁻¹⁰ nanowires,¹¹⁻¹³ nanobelts¹⁴⁻¹⁷ and nanotubes¹⁸⁻²⁰ were successfully prepared and exhibited excellent performances in different applications due to their morphology related effect in both physical and chemical properties. For example, CuV_2O_6 nanowires showed higher discharge capacity and enhanced electrode kinetics compared with the bulk particles due to the larger surface area and shorter diffusion route for lithium intercalation.²¹ Therefore, the controllable preparation of the transition-metal vanadates 1-D nanostructures with specific morphologies is of great interest in recent years.

As a typical transition-metal vanadate, iron vanadate (FeV_xO_y) shows very good performances in high energy density lithium batteries,²²⁻²⁵ sensors²⁶ and catalysis.^{27, 28} Since all those applications seriously relate to the morphologies and surface area of the FeV_xO_y nanostructure, it is expected that porous 1-D nanostructures with large surface area could be beneficial to the performances. For example, porous FeVO_4 nanorods as a sensor material exhibited higher selectivity and sensitivity toward n-butanol compared with FeVO_4 nanoparticles, attributed to the high surface area and porosity.²⁹ Porous FeVO_4 nanorods were usually prepared through a hydrothermal method.^{29, 30} According to this method, FeVO_4 nanorods with lattice water were first obtained after the hydrothermal reactions, while the porous structures formed during the subsequent heat treatment. The lengths of the FeVO_4 nanorods were normally in the range of 1-4 μm , while the pore sizes were hard to control. To take full advantages of the FeV_xO_y 1-D nanostructures in the applications of lithium batteries, sensors and catalysis, it is desirable to controllably

synthesize FeV_xO_y 1-D nanostructures with a broader range in lengths and pore sizes.

In this work, we developed a simple hydrothermal method to controllably synthesize porous FeV_xO_y 1-D nanostructures. On behalf of the new method, the lengths of the porous FeV_xO_y 1-D nanostructures could be tuned from several micrometers to several millimeters, while the pore sizes were also tuned meanwhile. The mechanisms of formation and controllable growth of porous FeV_xO_y 1-D nanostructures were also systematically studied. Finally, we tested the activity and stability of the porous FeV_xO_y 1-D nanostructures in the new developed application of selective catalytic reduction (SCR) of NO with NH_3 .³¹

Experimental

Synthesis of FeV_xO_y 1-D nanostructures

All the reagents were purchased from Sinopharm Chemical Reagent Company and were used without further purification.

The FeV_xO_y 1-D nanostructures were prepared through a modified hydrothermal method.³⁰ In a typical process, 1.5 mmol of NH_4VO_3 was first dissolved in 65 mL of HNO_3 aqueous solution (0.2 mol/L). 10 mL of $\text{Fe}(\text{NO}_3)_3 \cdot 9\text{H}_2\text{O}$ (0.075 mol/L) solution then was added. Thereafter, ammonium hydroxide was added to adjust the pH values. Yellow precipitates were appeared in this process. The obtained suspension was stirred for 0.5 h before it was transferred to a stainless steel reaction tank with polytetrafluoroethylene (PTFE) lining (100 mL) and maintained at 180 °C for 24 h. After reaction, the obtained precipitate was separated by centrifugation and was washed with water and ethanol for several times. Finally, the samples were dried at 80 °C for 12 h and calcined at 450 °C for 2 h in air. In the above process, the pH value is critical to the morphologies of the FeV_xO_y 1-D nanostructures. The samples prepared at pH values of 4.0, 5.0 and 6.0 were

denoted as FeV_xO_y -4, FeV_xO_y -5 and FeV_xO_y -6 before heat treatment, while as A- FeV_xO_y -4, A- FeV_xO_y -5 and A- FeV_xO_y -6 after heat treatment, respectively.

Characterization

The morphologies were observed by a scanning electron microscopy (SEM, JEOL, JSM-6700F), a transmission electron microscope (TEM, JEM-200CX) and a field emission high resolution transmission electron microscope (HRTEM, JEM-2100F). Powder X-ray diffraction (XRD) was performed with a Rigaku D/MAX-RB X-ray diffractometer by using $\text{Cu K}\alpha$ (40 kV, 40 mA) radiation and a secondary beam graphite monochromator. Nitrogen adsorption-desorption isotherms of the samples were measured at -196°C using an ASAP 2010 Micromeritics. The specific surface area of the samples was calculated by the Brunauer-Emmett-Teller (BET) method. Thermogravimetric analysis (TGA, SHIMADZU DTG-60H) was used to investigate the thermal decomposition behavior of the samples. The temperature was increased from room temperature to 900°C at a rate of $10^\circ\text{C min}^{-1}$.

Catalytic activity measurements

The SCR activities were tested in a fixed-bed quartz micro-reactor (i.d. 7 mm) operating in a steady state flow mode. The typical reactant conditions were as follows: 0.4g catalysts (40-60 mesh), 550 ppm NO , 550 ppm NH_3 , 3% O_2 , 10% H_2O (when used) and balance N_2 . The total flow rate was 250 mL/min leading to a gas

hourly space velocity (GHSV) of 20000 h^{-1} . The temperature was increased from 100 to 400°C step by step. At each temperature step the concentrations of NO , N_2O and NH_3 were recorded when the SCR reaction reached steady state after 15 min. The concentrations of NO in the inlet and outlet gases were measured by a KM9106 flue gas analyzer. The concentrations of N_2O and NH_3 were measured by a Transmitter IR N_2O analyzer and IQ350 ammonia analyzer.

Results and discussion

FeV_xO_y 1-D nanostructures (without annealing) with different lengths were synthesized by a hydrothermal method through simply adjusting the pH values of the precursors. FESEM images (Fig. 1a-f) show that uniform FeV_xO_y 1-D nanostructures are obtained after the hydrothermal reactions. It is obvious that the lengths of the as-prepared 1-D nanostructures increase with the increase of pH values. Fig. 1g further summarizes that the lengths of FeV_xO_y 1-D nanostructures can be tuned from several micrometers (nanorods) to several millimeters (nanowires) with the ratio of length/diameter increasing from about 10 to more than 1000, when the pH value increased from 4.0 to 6.0. More interestingly, those long nanowires (FeV_xO_y -6) were automatically weaved to a fabric after the hydrothermal reactions as shown in the inset of Fig. 1c. This property makes the nanowires very easy to be separated and cleaned after hydrothermal reactions.

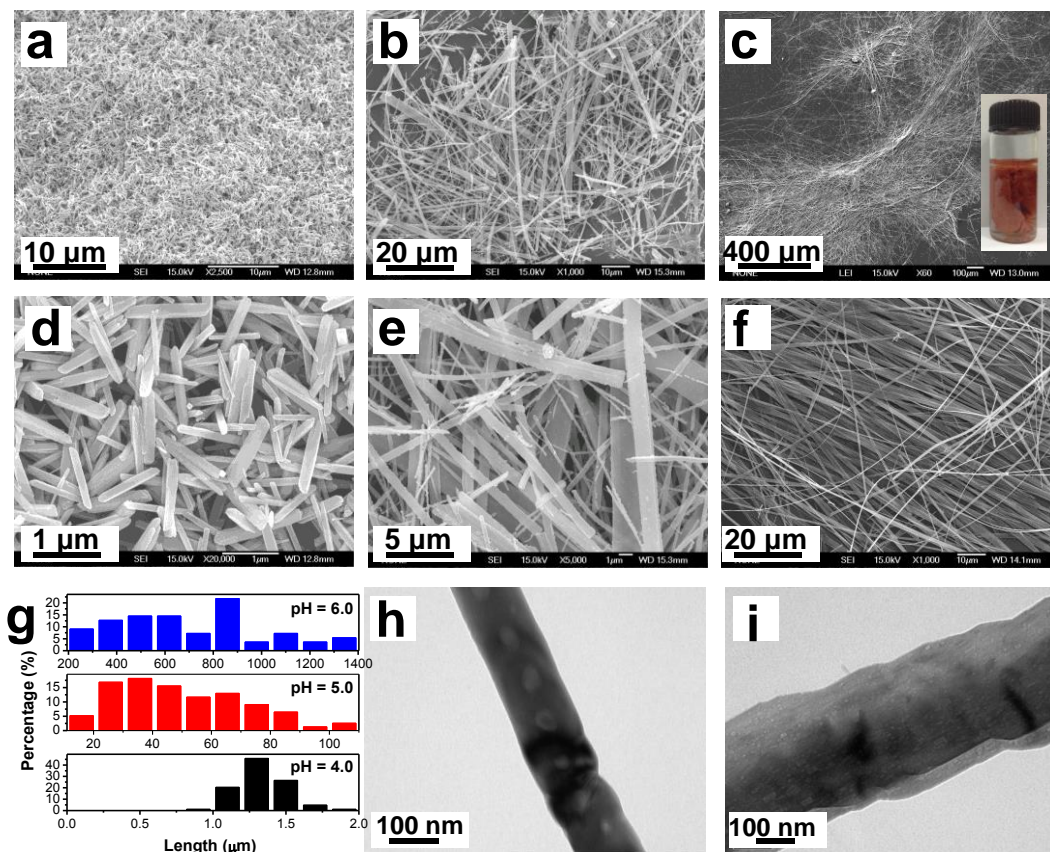


Fig. 1 FESEM images of the FeV_xO_y 1-D nanostructures prepared at different pH values of (a and d) 4.0, (b and e) 5.0 and (c and f) 6.0. (g) is the statistical length distribution of the FeV_xO_y 1-D nanostructures estimated from the FESEM images. (h) and (i) are the TEM images of A- FeV_xO_y -4 and A- FeV_xO_y -6 1-D nanostructures, respectively. The inset in (c) is the optical image of FeV_xO_y -6.

Cite this: DOI: 10.1039/c0xx00000x

www.rsc.org/xxxxxx

ARTICLE TYPE

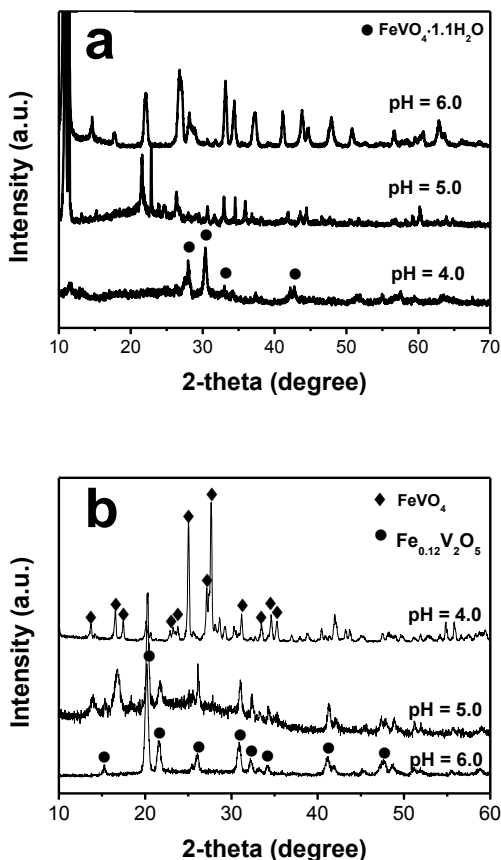


Fig. 2 XRD patterns of the FeV_xO_y 1-D nanostructures obtained at different pH conditions before (a) and after (b) heat treatment.

Table 1 A summary of the molecular structure, length, BET surface area and mean pore sizes of the FeV_xO_y 1-D nanostructures prepared at different pH values.

Samples	pH values	Molecular structure (annealed)	Mean Length (μm)	BET surface area (m^2/g)	Mean Pore size (nm)
1	4.0	FeVO_4	1.33	16.279	16.68
2	5.0	$\text{Fe}_{0.18}\text{V}_2\text{O}_5$	50.12	46.138	15.85
3	6.0	$\text{Fe}_{0.18}\text{V}_2\text{O}_5$	706.77	105.565	8.72

Thermal treatment was applied to further crystallize the as-prepared FeV_xO_y 1-D nanostructures after hydrothermal reactions. The morphologies of the uniform nanorods (A- FeV_xO_y -4) and ultralong nanowires (A- FeV_xO_y -6) after annealing are shown in Fig. S1. Fig. S1a and b indicate that the surfaces of the annealed FeV_xO_y 1-D nanostructures become rough after annealing. TEM images (Fig. 1h and i) and HRTEM images (Fig. S2) further indicate that pores are formed during the annealing process. The mean pore sizes of

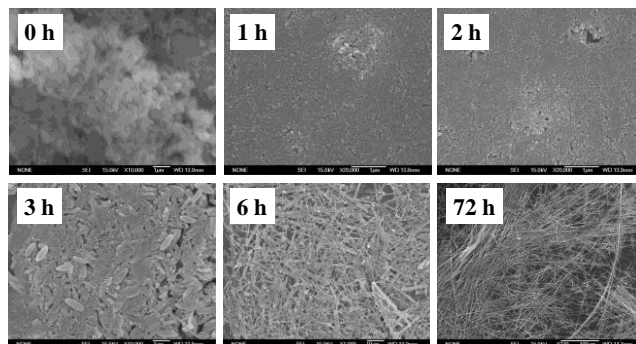
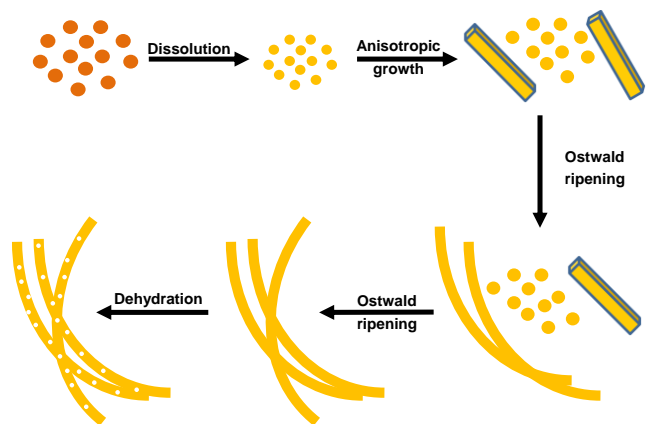


Fig. 3 Morphological evolution of FeV_xO_y -6 1-D nanostructure at different synthesis stages, starting from the precursor nanoparticles 0h and followed by 1h, 2h, 3h, 6h and 72 h hydrothermal treatment of the precursors

the A- FeV_xO_y 1-D nanostructures estimated from the (HR)TEM images (Fig. 1 and Fig. S2) are summarized in Table 1. It is indicated that the pore sizes decrease with the increase of pH values, A- FeV_xO_y -6 has the smallest pore size. Table 1 also indicates that the surface areas of the A- FeV_xO_y 1-D nanostructures determined by N_2 adsorption-desorption isotherms increase with the increase of pH values. The thermal analysis (Fig. S3a) indicates that both FeV_xO_y -4 and FeV_xO_y -6 have two obvious steps of weight loss ranging from 100 to 240 $^\circ\text{C}$ and 240 to 400 $^\circ\text{C}$, which are corresponding to two steps of water molecules loss. Obviously, FeV_xO_y -6 has much more lattice water than FeV_xO_y -4. XRD pattern (Fig. 2a) confirm that the FeV_xO_y -4 is in the form of $\text{FeVO}_4 \cdot 1.1\text{H}_2\text{O}$. The number of lattice water is coincident well with the number calculated from the TG results. Unfortunately, the molecular formula of FeV_xO_y -5 and FeV_xO_y -6 are hard to be determined according to the present data.

The DSC analysis (Fig. S3b) shows that an obvious endothermic peak exists at about 400 $^\circ\text{C}$ indicating the crystallization of the FeV_xO_y nanostructures. Accordingly, the FeV_xO_y nanostructures could be fully crystallized at the temperature of 450 $^\circ\text{C}$. XRD patterns (Fig. 2b) confirm that A- FeV_xO_y -4 is mainly in the form of FeVO_4 (JCPDS-ICDD Card No. 38-1372), while both A- FeV_xO_y -5 and A- FeV_xO_y -6 are mainly in the form of $\text{Fe}_{0.12}\text{V}_2\text{O}_5$ (JCPDS-ICDD Card No. 49-0805). Combined with the molecular formula and the TG results (Fig. S3a), the number of lattice water for FeV_xO_y -6 then is estimated to be about 2.1. Besides, the above result indicates that the FeV_xO_y samples lost the lattice water and are fully crystallized after annealing at 450 $^\circ\text{C}$ for 2h, although their crystalline structures are different.

Combined with the (HR)TEM, TG and XRD results, it can be deduced that the formation of pores in the FeV_xO_y 1-D nanostructures is possibly due to the loss of lattice water. FeV_xO_y -5 and FeV_xO_y -6 own much more lattice water than that of FeV_xO_y -4, hence have much more pores and larger pore volumes than that of



Scheme 1 Schematic illustration of the processes occurring at different stages which lead to the formation of FeV_xO_y ultralong nanowires.

FeV_xO_y -4 after annealing. The different pore size distribution was probably attributed to the different molecular formulae. The exact reason needs further investigation.

To understand the formation process of FeV_xO_y 1-D nanostructures, the evolution of FeV_xO_y morphologies with different hydrothermal durations was studied. Fig. 3 shows that the initial FeV_xO_y -6 before hydrothermal reactions is in the form of particles with the diameters of several micrometers. The particles first become smaller (several nanometers) and then regrow to dozens of nanometers after 1.0 h and 2.0 h of hydrothermal reactions, respectively.

When the growth time increases to 3.0 h, nanorods even small amount of nanowires with length up to dozens of micrometers start to appear with the coexistence of nanoparticles. With the reaction going on, the amount of nanoparticles continuously decreases while the amount of nanowires increase and the shape of the nanowires become more and more regular. Pure and regular nanowires could be obtained after 72 h of reactions. Obviously, this phenomenon corresponds to a typical ‘‘Ostwald Ripening’’ process contained the dissolving of small nanoparticles and the linear growth of nanowires. The corresponding XRD patterns (Fig. S4) further confirm that the initial FeV_xO_y -6 are amorphous (0.0 h) and start to crystallize (3.0 h) with the appearance of nanorods and nanowires, and are fully crystallized to form hydrates (72.0 h) during the hydrothermal process. Similar process was also observed for the growth of FeV_xO_y -4 (Fig. S5).

Based on the above results, the formation process of porous FeV_xO_y 1-D nanostructure could be summarized into four steps as illustrated in Scheme 1. First, the vanadates in the form of amorphous particles are dissolved into smaller nanoparticles under the hydrothermal condition. Second, the formed nanoparticles start to regrow orientationally, nanorods and short nanowires appear in this stage. Third, the ‘‘ostwald-ripening’’ process makes the small nanoparticles continuously dissolve and the FeV_xO_y 1-D nanostructure linearly grows. Pure nanorods and nanowires are obtained. Finally, the porous structures were derived from the loss of lattice water during the heat treatment.

It is obvious that the lengths of the FeV_xO_y 1-D nanostructures are governed by the pH values. In this work, the pH values of the precursors are mainly adjusted by the HNO_3 aqueous solution and ammonium hydroxide. Here the HNO_3 aqueous solution is used to favor the dissolution of NH_4VO_3 and meanwhile expand the pH value range to

acidic condition for hydrothermal reaction. To further investigate the influences of pH values on the morphologies of FeV_xO_y . The pH values were further adjusted to 2.0 and 7.0, respectively. Fig. S6 indicates that a mixture of irregular nanosheets and nanorods were obtained when the pH value was decreased to 2.0 (Fig. S6a). Only FeV_xO_y nanoparticles were observed when the pH value was increased to 7.0 (Fig. S6b). It then can be summarized that the FeV_xO_y nanostructures are favorable to transfer from higher dimension (2-D nanosheets) to lower dimension (1-D nanorods and nanowires) and even to zero-dimension (nanoparticles) with the pH values increase from 2.0 to 7.0.

The transfer of 2-D to 0-D nanostructure can be connected with the change of driven force of nucleation and growth rate. It's well known that low dimensional nanostructures are favorable to form at substantially slow nucleation and growth rate, since the final product of the nanoparticles could take a range of shapes deviated from the thermodynamic ones when the growth rate turns into kinetic control.³⁴⁻³⁷ In our experiments, FeV_xO_y particles were formed before hydrothermal reactions, the driven force of nucleation and growth rate mainly depended on the rate of dissolve and regrowth of FeV_xO_y as demonstrated in the formation mechanism above. It is understandable that FeV_xO_y is much easier to dissolve to get higher concentrations of Fe^{3+} and VO_x^{3-} ions in solution at lower pH values, which means that the rates of dissolve and regrowth are higher at lower pH values. This is coincident with the above results that lower dimensional nanostructures occurred at lower nucleation and growth rate with the increasing of pH values. Therefore, we propose that the morphologies of FeV_xO_y , especially the lengths of FeV_xO_y 1D nanostructures, are mainly determined by the driven force of nucleation and growth rate.

As a new developed application, FeVO_4 was reported to be a promising NH_3 -SCR catalyst for NO_x removal in the medium temperature range.³¹ Moreover, since FeVO_4 has a much higher melting point (ca. 850 °C) than that of V_2O_5 (ca. 690 °C) which is the active component of the commercialized catalyst.³¹ Therefore, FeVO_4 possesses higher thermal stability and benefits for the NO_x removal from diesel engines.

In this work, we chose A- FeV_xO_y -4 (FeVO_4 nanorods) which has the best mechanical strength to explore the application for SCR reaction of NO. Fig. 4a shows that the temperature window (the temperature range at which the conversion of NO is higher than 80%) ranges from 200 to 400 °C and the selectivity towards N_2 is above 98% over the whole temperature range (Fig. S7). This result is quite important in NO_x removal at low to medium temperatures. It was also found that the activity of A- FeV_xO_y -4 was quite stable in 20 h (Fig. 4b), and the porous structure also remained after the long duration reactions (Fig. 4c).

Since a large amount of H_2O (2–15 vol%) and certain amounts of SO_2 (30–2000 ppm) usually exist in the exhaust and the adsorption of water and SO_2 on the catalyst surface may poison the catalyst, the effect of H_2O and SO_2 on NO conversion over A- FeV_xO_y -4 was further studied with a feed stream containing 10 vol% H_2O and 200 ppm SO_2 . Fig. 4b shows that the simultaneous addition and removal of H_2O and SO_2 almost didn't change the NO_x conversion. This result demonstrates that A- FeV_xO_y -4 is highly resistant and reversible to both SO_2 and H_2O . It has been demonstrated that the high NH_3 -SCR activity and $\text{H}_2\text{O}/\text{SO}_2$ durability of $\text{FeVO}_4/\text{TiO}_2$ catalyst was attributed to the surface enriched VO_x species on the FeVO_4 phase. The observed high N_2

selectivity was attributed to the presence of electronic inductive effect between Fe^{3+} and V^{5+} , thus effectively decreasing the unwanted NH_3 unselective oxidation at high temperatures.³¹ We believe the VO_x species and the $\text{Fe}^{3+}\text{-O-V}^{5+}$ linkages played the similar roles to achieve high $\text{NH}_3\text{-SCR}$ activity, $\text{H}_2\text{O}/\text{SO}_2$ durability and high N_2 selectivity as demonstrated in this work. Obviously, the porous structure with large surface area could provide enough active sites for the reactions. Therefore, the porous FeVO_4 nanorods are a promising candidate for the de- NO_x catalysts.

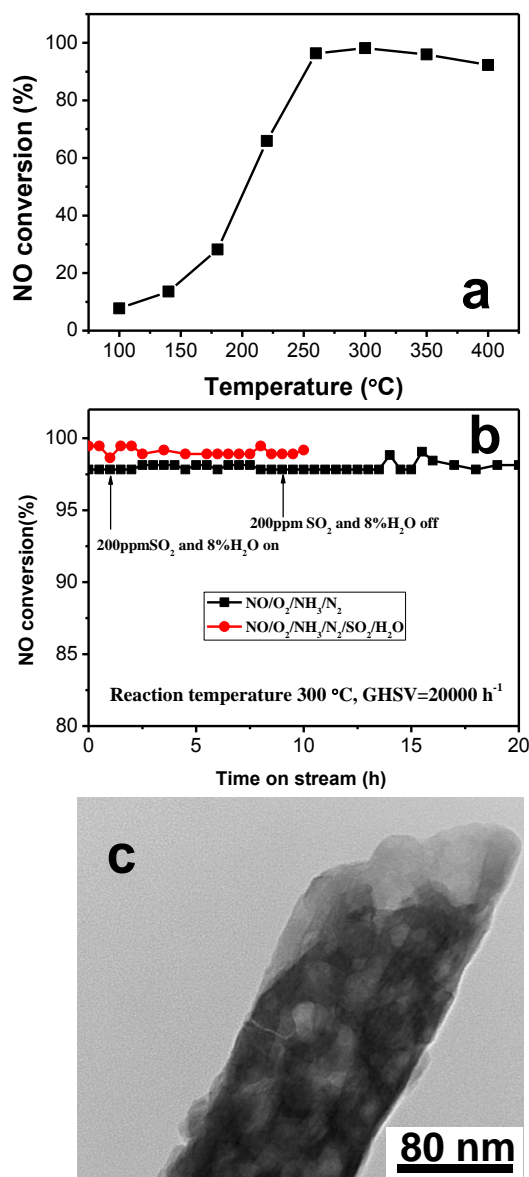


Fig. 4 a) NO conversion as a function of temperature in the feed gas of 250 mL/min total rate, 500ppm NO, 500ppm NH_3 , 3% O_2 , and N_2 balance, $\text{GHSV}=20000\text{h}^{-1}$. b) Stability test at 300 °C for 20 h (black solid square) and $\text{SO}_2/\text{H}_2\text{O}$ durability test (red solid circle) in the feed gas of 250 mL/min total rate, 500ppm NO, 500ppm NH_3 , 3% O_2 , and N_2 balance, $\text{GHSV}=20000\text{h}^{-1}$. 200ppm SO_2 and 8% H_2O were introduced for the $\text{SO}_2/\text{H}_2\text{O}$ durability test. c) TEM images of the used porous A- FeV_xO_y -4 sample after 20 h of stability test.

20 Conclusions

In this work, porous FeV_xO_y 1-D nanostructures with different lengths were controllably synthesized through a hydrothermal method. The length could be tuned from several micrometers to several millimeters simply increasing the pH value from 4.0 to 6.0. The formation process of the porous FeV_xO_y 1-D nanostructures can be summarized into three steps, namely dissolve, anisotropic growth, ostwald ripening and dehydration. In this process, the driven force of nucleation and growth rate could be tuned by the pH values thus changing the morphologies of FeV_xO_y nanostructures. It was found that the pore sizes decrease with the increase of pH values while the surface areas increase with the increase of pH values. The porous FeVO_4 nanorods were found very active and stable in the application of SCR of NO with NH_3 . We believe that the porous FeV_xO_y 1-D nanostructures with different lengths are also interested in other applications like lithium batteries and sensors.

Acknowledgements

This work was financially supported by National Natural Science Foundation of China (21303099 & 51108258), Research Fund for the Innovation Program of Shanghai University (K.10040713003), Shanghai Municipal Education Commission (B.37040713001) and Dongguan Municipal Research Program for Colleges and Institutes (Dongke [2012]123, No. 201210825000535).

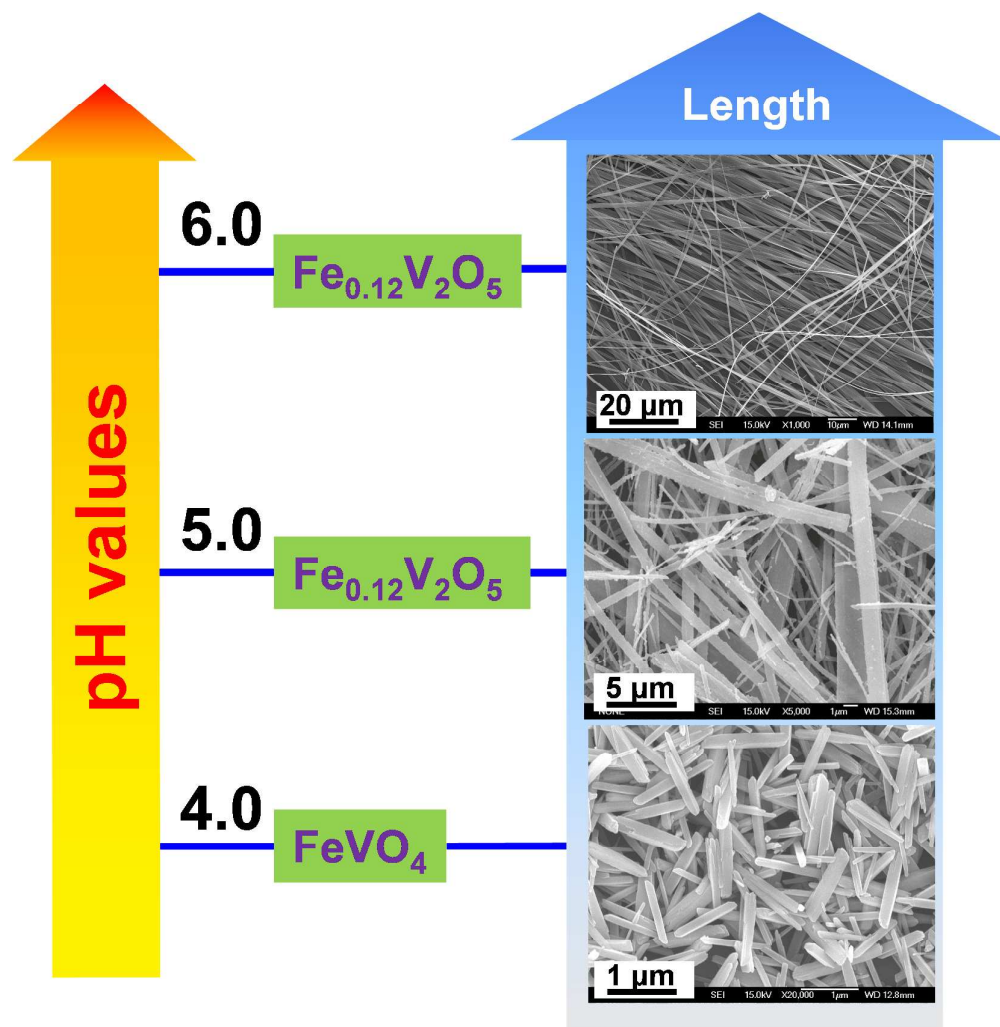
Notes and references

- *Research Center of Nano Science and Technology, Shanghai University, Shanghai 200444, P. R. China. Fax: +86-21-66136079; Tel: +86-21-66136081; E-mail: dszhang@shu.edu.cn
- Electronic Supplementary Information (ESI) available: SEM, HRTEM, XRD, TG, DSC results of the FeV_xO_y sample. See DOI: 10.1039/b000000x/
- S. S. Liu, F. Hu, J. Zhang, H. X. Tang and M. W. Shao, *ACS Appl. Mater. Interfaces*, 2013, **5**, 3208-3211.
 - V. Soenen, J. M. Herrmann and J. C. Volta, *J. Catal.*, 1996, **159**, 410-417.
 - Y. N. Kozlov, V. B. Romakh, A. Kitaygorodskiy, P. Buglyo, G. Suss-Fink and G. B. Shul'pin, *J. Phys. Chem. A*, 2007, **111**, 7736-7752.
 - R. G. Li, F. X. Zhang, D. G. Wang, J. X. Yang, M. R. Li, J. Zhu, X. Zhou, H. X. Han and C. Li, *Nat. Commun.*, 2013, **4**, 1432.
 - H. Y. Xu, H. Wang, Z. Q. Song, Y. W. Wang, H. Yan and M. Yoshimura, *Electrochim. Acta*, 2004, **49**, 349-353.
 - B. Yan, S. P. Wang, H. X. Yang, L. J. Feng, H. Y. Wei and Y. Z. Yang, *Asian J. Chem.*, 2013, **25**, 4315-4318.
 - S. Eda, M. Fujishima and H. Tada, *Appl. Catal. B-Environ.*, 2012, **125**, 288-293.
 - D. P. Singh, K. Polychronopoulou, C. Reholz and S. M. Aouadi, *Nanotechnology*, 2010, **21**, 325601.
 - L. Z. Pei, Y. Q. Pei, Y. K. Xie, C. G. Fan and H. Y. Yu, *Crystengcomm*, 2013, **15**, 1729-1738.
 - S. J. Lei, K. B. Tang, Y. Jin and C. H. Chen, *Nanotechnology*, 2007, **18**, 175605.
 - W. Hu, X. B. Zhang, Y. L. Cheng, C. Y. Wu, F. Cao and L. M. Wang, *ChemSusChem*, 2011, **4**, 1091-1094.

12. M. Shahid, I. Shakir, H. Yang, P. Rai and D. J. Kang, *Mater. Chem. Phys.*, 2011, **131**, 184-189.
13. M. Shahid, A. Nafady, I. Shakir, U. A. Rana, M. Sarfraz, M. F. Warsi, R. Hussain and M. N. Ashiq, *J. Nanopart. Res.*, 2013, **15**, 1826.
14. J. G. Yu, J. C. Yu, W. K. Ho, L. Wu and X. C. Wang, *J. Am. Chem. Soc.*, 2004, **126**, 3422-3423.
15. C. J. Mao, X. J. Wang, X. Wu, J. J. Zhu and H. Y. Chen, *Nanotechnology*, 2008, **19**, 035607.
16. S. W. Liu, W. Z. Wang, L. Zhou and L. S. Zhang, *J. Cryst. Growth*, 2006, **293**, 404-408.
17. L. F. Bai, J. B. Zhu, X. D. Zhang and Y. Xie, *J. Mater. Chem.*, 2012, **22**, 16957-16963.
18. Y. Wang and G. Z. Cao, *J. Mater. Chem.*, 2007, **17**, 894-899.
19. H. J. Muhr, F. Krumeich, U. P. Schonholzer, F. Bieri, M. Niederberger, L. J. Gauckler and R. Nesper, *Adv. Mater.*, 2000, **12**, 231-232.
20. J. Cao, J. Choi, J. L. Musfeldt, S. Lutta and M. S. Whittingham, *Chem. Mat.*, 2004, **16**, 731-736.
21. H. Ma, S. Y. Zhang, W. Q. Ji, Z. L. Tao and J. Chen, *J. Am. Chem. Soc.*, 2008, **130**, 5361-5367.
22. D. H. Sim, X. H. Rui, J. Chen, H. T. Tan, T. M. Lim, R. Yazami, H. H. Hng and Q. Y. Yan, *RSC Adv.*, 2012, **2**, 3630-3633.
23. S. Patoux and T. J. Richardson, *Electrochem. Commun.*, 2007, **9**, 485-491.
24. S. R. Li, N. Yesibolati, Y. Qiao, S. Y. Ge, X. Y. Feng, J. F. Zhu and C. H. Chen, *J. Alloy. Compd.*, 2012, **520**, 77-82.
25. S. Denis, R. Dedryvere, E. Baudrin, S. Laruelle, M. Touboul, J. Olivier-Fourcade, J. C. Jumas and J. M. Tarascon, *Chem. Mat.*, 2000, **12**, 3733-3739.
26. G. Mangamma, E. Prabhu and T. Gnanasekaran, *Bull. Electrochem.*, 1996, **12**, 696-699.
27. K. Routray, W. Zhou, C. J. Kiely and I. E. Wachs, *ACS Catal.*, 2011, **1**, 54-66.
28. J. H. Deng, J. Y. Jiang, Y. Y. Zhang, X. P. Lin, C. M. Du and Y. Xiong, *Appl. Catal. B-Environ.*, 2008, **84**, 468-473.
29. Y. V. Kaneti, Z. J. Zhang, J. Yue, X. C. Jiang and A. B. Yu, *J. Nanopart. Res.*, 2013, **15**, 1948.
30. H. Ma, X. J. Yang, Z. L. Tao, J. Liang and J. Chen, *Crystengcomm*, 2011, **13**, 897-901.
31. F. Liu, H. He, Z. Lian, W. Shan, L. Xie, K. Asakura, W. Yang and H. Deng, *J. Catal.*, 2013, **307**, 340-351.
32. E. Baudrin, S. Denis, F. Orsini, L. Seguin, M. Touboul and J. M. Tarascon, *J. Mater. Chem.*, 1999, **9**, 101-105.
33. E. Baudrin, S. Laruelle, S. Denis, M. Touboul and J. M. Tarascon, *Solid State Ion.*, 1999, **123**, 139-153.
34. X. Liang, X. Wang, Y. Zhuang, B. Xu, S. M. Kuang and Y. D. Li, *J. Am. Chem. Soc.*, 2008, **130**, 2736-2737.
35. Z. B. Zhuang, Q. Peng and Y. D. Li, *Chem. Soc. Rev.*, 2011, **40**, 5492-5513.
36. Y. J. Xiong, J. M. McLellan, J. Y. Chen, Y. D. Yin, Z. Y. Li and Y. N. Xia, *J. Am. Chem. Soc.*, 2005, **127**, 17118-17127.
37. Y. J. Xiong and Y. N. Xia, *Adv. Mater.*, 2007, **19**, 3385-3391.

55

Graphical abstract



org

The length of porous FeV_xO_y 1-D nanostructures could be tuned from several micrometers to several millimeters.